ARTICLE

Photodissociation Spectra of OCS^+ via $B^2\Sigma^+ \leftarrow X^2\Pi$ Transitions

Dan-na Zhou, Li-min Zhang*, Lin Chen, Dan Wu

Department of Chemical Physics, University of Science and Technology of China, Hefei 230026, China

(Dated: Received on March 25, 2013; Accepted on May 3, 2013)

In the wavelength range of 231−275 nm, we have studied the mass-resolved dissociation spectra of OCS^+ via $B^2\Sigma^+ \leftarrow X^2\Pi_{3/2}(000)$ and $B^2\Sigma^+ \leftarrow X^2\Pi_{1/2}(000,\ 001)$ transitions by preparing OCS^+ ions in the well-defined spin-orbit states. The spectroscopic constants of ν_1(CS stretch)=828.9 (810.4) cm^{-1}, ν_2(bend)=491.3 cm^{-1} and ν_3(CO stretch)=1887.2 cm^{-1} for $OCS^+(B^2\Sigma^+)$ are deduced. The observed dependence of the ν_2(bend) mode excitation of $B^2\Sigma^+$ on the spin-orbit splitting of $X^2\Pi(\Omega=1/2,\ 3/2)$ in the $B^2\Sigma^+ \leftarrow X^2\Pi$ transition can be attributed to the K coupling between the $(000)^2\Pi_{1/2}$ and $(010)^2\Sigma^+_{1/2}$ vibronic levels of $X^2\Pi$ state, which makes the $B^2\Sigma^+(010) \leftarrow X^2\Pi_{1/2}(000)$ transition possible.

Key words: OCS^+, Photodissociation, Bending vibration mode, K coupling

I. INTRODUCTION

The linear triatomic OCS^+ ion is one of the ideal molecules for the detailed exploration of fundamental physical processes including Fermi resonance, the Renner-Teller effect, and spin-orbit interactions [1, 2]. The vibronic structures of $OCS^+(X^2\Pi,\ A^2\Pi,\ B^2\Sigma^+$ and $C^2\Sigma^+)$ have been investigated by various experimental techniques [3−27], including photoelectron [3−9], vacuum ultraviolet (VUV) pulsed field ionization-photoelectron (PFI-PE) [10, 11], photoionization efficiency [12], laser-induced fluorescence emission [13, 14], photon dissociation measurements [15−20], and resonance-enhanced multiphoton ionization (REMPI) of the neutral OCS [21−24]. In comparison with the extensive works for the $OCS^+(A^2\Pi)$ state, only a few laser spectroscopic studies about the $OCS^+(B^2\Sigma^+)$ state were reported. Kakoschke *et al.* performed the first experiment on the one photon dissociation spectroscopy of OCS^+ via the $B^2\Sigma^+/A^2\Pi \leftarrow X^2\Pi$ transitions in 1985 by using tunable laser and duoplasmatron ion source [17]. Liu *et al.* demonstrated a time-sliced velocity imaging technique to study the mode-selected predissociation of $OCS^+(B^2\Sigma^+)$ ion via the $B^2\Sigma^+ \leftarrow X^2\Pi_{1/2}$ excitation by preparing OCS^+ in the $X^2\Pi_{1/2}$ state via [2+1] multiphoton ionization of OCS molecules [25, 26].

In this work, we investigate the vibrational levels of $OCS^+(B^2\Sigma^+)$ involving one quantum of bending mode by measuring the $B^2\Sigma^+ \leftarrow X^2\Pi_{1/2,3/2}$ dissociation spectra of OCS^+. Especially, we attempt to learn the dependence of the bending mode excitation of $OCS^+(B^2\Sigma^+)$ on the spin-orbit splitting of $OCS^+(X^2\Pi)$ in the $B^2\Sigma \leftarrow X^2\Pi$ transition, where the $B^2\Sigma^+$ state, differing from $A^2\Pi$, has no spin-orbit splitting.

II. EXPERIMENTS

The experimental setup has been reported previously [28]. The jet-cooled OCS molecules were produced by the supersonic expansion of a mixing OCS/He gas (total pressure 3.5 mPa, OCS/He≈20%) through a pulsed nozzle (General Valve) with a nozzle orifice diameter of 0.5 mm into a photoionization chamber. The output of the ionization dye laser (about 2 mJ/pulse) was focused perpendicularly on the molecular beam of OCS by a quartz lenses with f=149 mm to produce OCS^+ ion via [3+1] resonance enhanced multi-photon ionization of OCS molecules. The dissociation dye laser (231−275 nm, 20−110 μJ/pulse) coaxially counterpropagated with the ionization laser was focused by another quartz lenses with f=291 mm to excite the OCS^+ ions. Both dye lasers were temporally and spatially matched with each other at the laser-molecular interaction point. The wavelength of the laser was calibrated using a wavemeter.

The ions were extracted and accelerated into a TOF (time of flight) mass spectrometer and drifted along a 70 cm long TOF tube, and finally detected by a microchannel plate (MCP) detector. The signals from the MCP output were amplified with a preamplifier (Stanford model SR240A). The mass-resolved data were collected by averaging the amplified signals for selected mass species with a transient recorder and stored in a personal computer (PC). The intensities of the ionization laser and the dissociation laser were monitored simultaneously during the experiment.

*Author to whom correspondence should be addressed. E-mail: lmzha@ustc.edu.cn

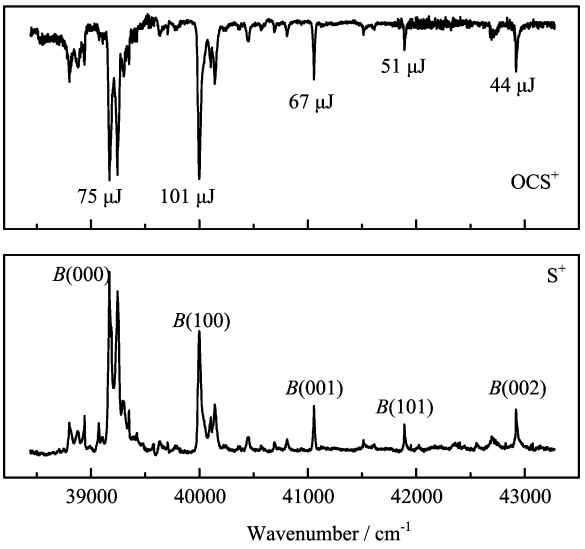

FIG. 1 The mass-resolved photodissociation spectra. The spectra are assigned to the $B^2\Sigma^+(v_1v_2v_3)\leftarrow X^2\Pi_{3/2}(000)$ vibronic transition of OCS^+. The energy per pulse of the dissociation laser was marked at the position of the resonance peaks in upper frame.

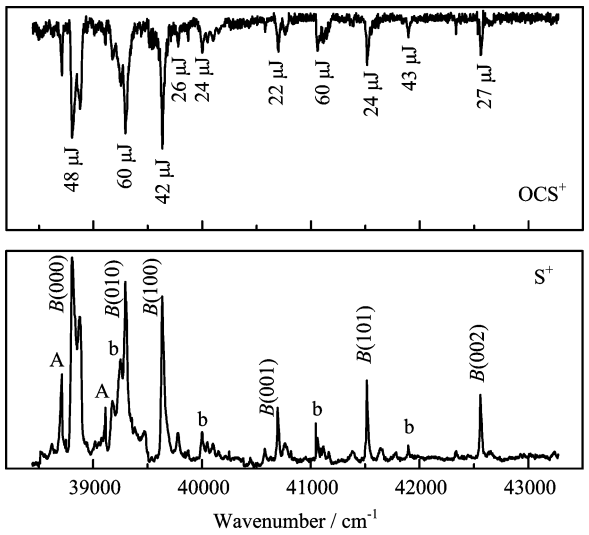

FIG. 2 The mass-resolved photodissociation spectra. The spectra are assigned to the $B^2\Sigma^+(v_1v_2v_3)\leftarrow X^2\Pi_{1/2}(000)$ vibronic transition of OCS^+. The marks "*A*" and "*b*" in the lower frame represent the bands assigned to the $A^2\Pi_{1/2}(v_1v_2v_3)\leftarrow X^2\Pi_{1/2}(000)$ transition and the $B^2\Sigma^+(v_1v_2v_3)\leftarrow X^2\Pi_{3/2}(000)$ transition, respectively.

III. RESULTS AND DISCUSSION

In this work, the OCS^+ ions were prepared in $X^2\Pi_{1/2}(000)$, $X^2\Pi_{3/2}(000)$, and $X^2\Pi_{1/2}(001)$ states with minimum amount of fragment ions by fixing the wavelengths of ionization laser at λ=420, 423, and 408.4 nm, respectively. The soft ionization at these wavelengths comes from the [3+1] REMPI process of OCS [21−24], which can be expressed as,

$$\mathrm{OCS}(X^1\Sigma^+(000))\xrightarrow{3h\nu}\mathrm{OCS}(E^1\Pi(000))\xrightarrow{h\nu}\mathrm{OCS}^+(X^2\Pi_{3/2}(000))\quad(1)$$

$$\mathrm{OCS}(X^1\Sigma^+(000))\xrightarrow{3h\nu}\mathrm{OCS}(F^1\Pi(000))\xrightarrow{h\nu}\mathrm{OCS}^+(X^2\Pi_{1/2}(000))\quad(2)$$

$$\mathrm{OCS}(X^1\Sigma^+(000))\xrightarrow{3h\nu}\mathrm{OCS}(F,G(001))\xrightarrow{h\nu}\mathrm{OCS}^+(X^2\Pi_{1/2}(001))\quad(3)$$

Thus, the mass-resolved photodissociation spectra (the depletion spectrum of parent ion OCS^+ and the enhanced spectrum of fragment ion S^+) in Fig.1−Fig.3 were obtained by scanning the dissociation laser in the range of 231−275 nm. With the aid of the spectroscopy of OCS^+ reported in Ref.[11, 17], the photodissociation spectra could be assigned as the $B^2\Sigma^+(v_1v_2v_3)\leftarrow X^2\Pi_{3/2}(000)$, $B^2\Sigma^+(v_1v_2v_3)\leftarrow X^2\Pi_{1/2}(000)$, and $B^2\Sigma^+(v_1v_2v_3)\leftarrow X^2\Pi_{1/2}(001)$ transitions of OCS^+, where v_1, v_2, and v_3 represent the vibrational quantum numbers of ν_1 (CS stretching), ν_2 (bending), and ν_3 (CO stretching) modes, respectively. The assignments of the photodissociation spectra shown in Fig.1−Fig.3 are summarized in Tables I−III. The pulse energy per pulse of the dissociation laser is marked at the position of resonance peaks in upper frame of the Fig.1−Fig.3.

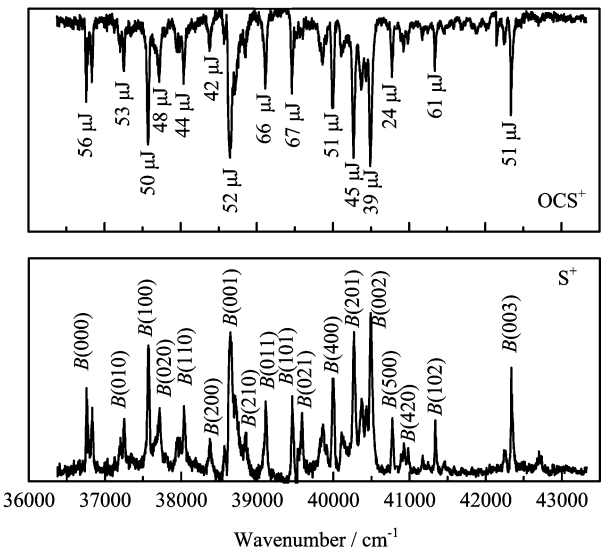

FIG. 3 The mass-resolved photodissociation spectra. The spectra are assigned to the $B^2\Sigma^+(v_1v_2v_3)\leftarrow X^2\Pi_{1/2}(001)$ vibronic transition of OCS^+.

The doublet feature of the $B^2\Sigma^+(000)$ band, with two lines separated by ∼72 cm^{-1}, is found in Fig.1−Fig.3.

DOI:10.1063/1674-0068/26/03/265-269

TABLE I Vibrational assignments for the $B^2\Sigma^+(v_1v_2v_3) \leftarrow X^2\Pi_{3/2}(000)$ bands of OCS^+.

$(v_1v_2v_3)$	$\nu_{exp,1}$[a]/cm^{-1}	$\Delta\nu$[a]/cm^{-1}	$\nu_{exp,2}$/cm^{-1}	$(\nu_{exp,1}-\nu_{exp,2})$/cm^{-1}	$\Delta\nu_{PFI}$[b]/cm^{-1}	$(\Delta\nu-\Delta\nu_{PFI})$/cm^{-1}
(000)	39170.8	0.0	39171 [17]	−0.2	0.0	0.0
(100)	39999.7	828.9	40000 [17]	−0.3	797.7	31.2
(001)	41057.2	1886.4			1876.9	9.5
(101)	41890.3	2719.5				
(002)	42920.5	3749.7			3729.5	20.2

[a] This work. $\Delta\nu$ values are energy measured with respect to $B^2\Sigma^+(000)$.
[b] Data of PFI-PE spectra from Ref.[12].

TABLE II Vibrational assignments for the $B^2\Sigma^+(v_1v_2v_3) \leftarrow X^2\Pi_{1/2}(000)$ bands of OCS^+.

$(v_1v_2v_3)$	$\nu_{exp,1}$[a]/cm^{-1}	$\Delta\nu$[a]/cm^{-1}	$\nu_{exp,2}$/cm^{-1}	$(\nu_{exp,1}-\nu_{exp,2})$/cm^{-1}	$\Delta\nu_{PFI}$[b]/cm^{-1}	$(\Delta\nu-\Delta\nu_{PFI})$/cm^{-1}
(000)	38806.1	0.0	38803.0 [17]	3.1	0.0 [12]	0.0
(010)	39295.5	489.4	39298.0 [17]	−2.5		
(100)	39635.0	828.9	39631.0 [17]	4.0	797.7 [12]	31.2
(001)	40696.3	1890.2			1876.9 [12]	13.3
(101)	41515.7	2709.6				
(002)	42558.9	3752.8			3729.5 [12]	23.3

[a] and [b] see Table I.

TABLE III Vibrational assignments (in cm^{-1}) for the $B^2\Sigma^+(v_1v_2v_3) \leftarrow X^2\Pi_{1/2}(001)$ bands of OCS^+.

$(v_1v_2v_3)$	ν_{exp}	$\Delta\nu$	$(v_1v_2v_3)$	ν_{exp}	$\Delta\nu$
(000)	36759.0	0	(101)	39460.4	2701.4
(010)	37253.1	494.1	(021)	39588.4	2829.4
(100)	37569.4	810.4	(400)	39990.4	3231.4
(020)	37718.1	959.1	(201)	40270.5	3511.5
(110)	38039.4	1280.4	(002)	40489.0	3730.0
(200)	38378.0	1619.0	(500)	40774.5	4015.5
(001)	38649.3	1890.3	(420)	40927.0	4168.0
(210)	38848.9	2089.9	(102)	41338.0	4579.0
(011)	39108.6	2349.6	(003)	42337.0	5578.0

Similar doublet structure of the $B^2\Sigma^+(000)$ band with a space of ∼30 cm^{-1} was also observed in previous PFI-PE spectra [11, 27]. The difference between the doublet splitting of ∼72 cm^{-1} in the this experiment and that of ∼30 cm^{-1} in the PFI-PE experiment [11, 27] may be attributed to the different excited ways of $OCS^+(B^2\Sigma^+)$. In this experiment, the doublet splitting is formed from the direct excitation of $B^2\Sigma^+(000) \leftarrow X^2\Pi(000)$. In the PFI-PE experiment the doublet splitting is formed from the decay (autoionization) of the super excitation state of neutral OCS molecule. However, the doublet structure of the $B^2\Sigma^+$ state cannot be ascribed to a fine structure splitting. We are not sure the origination of the doublet structure, and "a near resonant interaction" suggested in Ref.[11] is a possible interpretation for the doublet splitting of the $B^2\Sigma^+(000) \leftarrow X^2\Pi_{3/2}(000)$ transition in Fig.1. By selecting the lower component of the doublet as the origin of the $B^2\Sigma^+ \leftarrow X^2\Pi$ transition, the vibrationless electronic origin of the $B^2\Sigma^+ \leftarrow X^2\Pi_{3/2}(000)$ can be determined as 39170.8 cm^{-1}, which is in accordance with the value of 39171 cm^{-1} given in Ref.[17].

By relating the lowest excited level of a vibration mode to its vibration frequency, we can get the frequencies of three vibration modes from Tables I–III. It is found that the ν_1 value (CS stretch) of 810.4 cm^{-1} for the $B^2\Sigma^+ \leftarrow X^2\Pi_{1/2}(001)$ spectrum is 18.5 cm^{-1} lower than that for the $B^2\Sigma^+ \leftarrow X^2\Pi_{1/2,3/2}(000)$ spectra (828.9 cm^{-1}). This fact suggests that the transitions from the vibrational excited $X^2\Pi_{1/2}(001)$ level can make OCS^+ reach a position of the $B^2\Sigma^+$ potential surface related to a smaller ν_1 value along the CS stretching coordinate. In sum, the spectroscopic constants of ν_1(CS stretch)=828.9 (810.4) cm^{-1}, ν_2(bend)=491.3 cm^{-1}, and ν_3(CO stretch)=1887.2 cm^{-1} for $OCS^+(B^2\Sigma^+)$ are deduced from the data of the $B^2\Sigma^+(v_1v_2v_3) \leftarrow X^2\Pi$ transitions. In fact, we can use the data of the $B^2\Sigma^+ \leftarrow X^2\Pi_{1/2}(001)$ spectrum in Table III to fit out an entire set of spectral constants: ω_1=800.6 cm^{-1}, ω_2=484.4 cm^{-1}, ω_3=1884.5 cm^{-1}, x_{11}=1.4 cm^{-1}, x_{22}=−4.0 cm^{-1}, x_{33}=−9.2 cm^{-1}, x_{12}=−2.2 cm^{-1}, x_{13}=15.4 cm^{-1}, x_{23}=−13.1 cm^{-1}. By using this set of spectral constants, the maximum errors between the calculated wavenumbers and the experiment values in Table III are +8.1 and −9.0 cm^{-1}. The frequencies of

DOI:10.1063/1674-0068/26/03/265-269

the vibrational modes for $B^2\Sigma^+$ obtained in this work are in agreement with previous determinations [11, 17].

From the long $B^2\Sigma^+(v_100,\ v_1$=0, 1, 2, 4, 5) progression in the $B^2\Sigma^+\leftarrow X^2\Pi_{1/2}(001)$ spectrum of Fig.3, it is noticed that the $B(500)$-$B(400)$ gap of 784.1 cm^{-1} is obviously smaller than other $B(v_100)-B(v_1-1,0,0)$ gaps of 806.2−810.4 cm^{-1} for v_1=1, 2, 3, 4. We can attribute this rapid decreasing of the CS stretching frequency at v_1=5 to the larger anharmonicity of the potential energy surfaces (PES) of $OCS^+(B^2\Sigma^+)$ state. As pointed by Hirst [1], the $B^2\Sigma^+$ and $^4\Sigma^-$ states intersect over a wide range of CO distances when the CS distance is at about 1.7 Å, and the intersection seam lies at about 5000 cm^{-1} above the minimum of the $B^2\Sigma^+$ surface. Since the $B^2\Sigma^+(500)$ level at about 4400 cm^{-1} is near this intersection seam, it is possible that the interaction between the $^4\Sigma^-$ and $B^2\Sigma^+$ states increases the anharmonicity of PES of $OCS^+(B^2\Sigma^+)$ state, which makes the $B(500)$-$B(400)$ gap much smaller than other $B(v_100)$-$B(v_1-1,0,0)$ gaps (where v_1=1, 2, 3, 4).

In Fig.1 and Fig.2, the $B^2\Sigma^+\leftarrow X^2\Pi_{3/2}(000)$ and $B^2\Sigma^+\leftarrow X^2\Pi_{1/2}(000)$ spectra are very similar in spectral structure and in intensity distribution, except there is a frequency shift (the spin-orbit splitting of 364.5 cm^{-1} of $X^2\Pi$) between them. In principle, the excitation of the bending mode for $B^2\Sigma^+$ in the $B^2\Sigma^+\leftarrow X^2\Pi$ transition has a very low intensity, as a result of vanishing Franck-Condon factors. That is why no $B^2\Sigma^+(v_11v_3)$ band appears in the $B^2\Sigma^+\leftarrow X^2\Pi_{3/2}$ spectra. However, by observing the dissociation spectra in Fig.1−Fig.3, the $B^2\Sigma^+(v_11v_3)$ bands with v_2=1 appear remarkably in the $B^2\Sigma^+\leftarrow X^2\Pi(\Omega=1/2)$ spectra. No such band is seen in the $B^2\Sigma^+\leftarrow X^2\Pi_{3/2}(000)$ spectrum. Because the $B^2\Sigma^+$ state has no spin-orbit splitting, this observation suggests a dependence of the ν_2 mode excitation of $B^2\Sigma^+$ on the spin-orbit splitting of $X^2\Pi$. One should notice, that the energy gap of ∼360 cm^{-1} between 3/2 and 1/2 components of $X^2\Pi$ can hardly induce evident differences of the Franck-Condon factors between the $B^2\Sigma^+\leftarrow X^2\Pi(\Omega=3/2)$ and $B^2\Sigma^+\leftarrow X^2\Pi(\Omega=1/2)$ transitions. This argument is supported by both the similar spectral structures and similar intensity distributions in $B^2\Sigma^+\leftarrow X^2\Pi_{3/2}(000)$ and $B^2\Sigma^+\leftarrow X^2\Pi_{1/2}(000)$ spectra in Fig.1 and Fig.2 (except for the $B^2\Sigma^+(010)$ band with v_2=1). Hence, the vibronic levels of $X^2\Pi$ and their interaction should be important to determine the correlation between the bending ν_2 mode excitation of $B^2\Sigma^+$ and the spin-orbit splitting of $X^2\Pi$.

For a linear molecule $OCS^+(X^2\Pi)$ with v_2 bending quanta, the vibrational angular moment along molecular axis can have values $l_v\hbar$, where l_v=v_2, v_2-2, ...1, or 0. In view of the fact that the electronic orbital angular momentum of $OCS^+(X^2\Pi)$ has a nonzero projection of $\Lambda\hbar$ (Λ=1) along the molecular axis, the Renner-Teller coupling between Λ and l_v can form a new quantum number, $K=|\Lambda\pm l_v|$, corresponding to the vibronic components of $OCS^+(X^2\Pi)$ [10]. In this case, the vibronic levels of the $X^2\Pi$ state can be identified by the quantum number K, such as $(010)^2\Sigma^+_{1/2}$ and $(010)^2\Sigma^-_{1/2}$ levels with K=0, $(000)^2\Pi_{1/2}$ and $(000)^2\Pi_{3/2}$ levels with K=1, as well as $(010)^2\Delta_{3/2}$ and $(010)^2\Delta_{5/2}$ levels with K=2. The K coupling of two vibronic levels closed to each other has been found in many cases [10]. The smaller the energy gap of two vibronic levels is, the stronger the K coupling is. Referring to the calculated and observed vibronic levels of $OCS^+(X^2\Pi)$, it is found that the energy gap of ∼45 cm^{-1} between the $(000)^2\Pi_{1/2}$ and $(010)^2\Sigma^+_{1/2}$ vibronic levels is much smaller than that of ∼409 cm^{-1} between the $(000)^2\Pi_{3/2}$ and $(010)^2\Sigma^+_{1/2}$ vibronic levels [10]. Obviously, the former has a much stronger K coupling than the latter. Thus, the OCS^+ ions at $X^2\Pi_{1/2}(000)$ level can gain a finite bending vibration feature from the K coupling between the $(000)^2\Pi_{1/2}$ and $(010)^2\Sigma^+_{1/2}$ vibronic levels of the $X^2\Pi$ state, and the $B^2\Sigma^+(010)\leftarrow X^2\Pi_{1/2}(000)$ transition becomes possible by borrowing the intensity from the allowed $B^2\Sigma^+(010)\leftarrow X^2\Pi((010)^2\Sigma^+_{1/2})$ transition. Hence, it is not surprising that the notable $B^2\Sigma^+(010)\leftarrow X^2\Pi_{1/2}(000)$ band appears in the $B^2\Sigma^+\leftarrow X^2\Pi_{1/2}(000)$ spectrum while no such band is seen in the $B^2\Sigma^+\leftarrow X^2\Pi_{3/2}(000)$ spectrum.

In addition to the main bands for $B^2\Sigma^+(v_1v_2v_3)\leftarrow X^2\Pi_{1/2}(000)$ transitions, several weak vibrational bands, marked "b" in Fig.2, can be assigned to the $B^2\Sigma^+(v_1v_2v_3)\leftarrow X^2\Pi_{3/2}(000)$ transitions, because a small amount of $OCS^+(X^2\Pi_{3/2}(000))$ ions were produced in the prepareration of the $OCS^+(X^2\Pi_{1/2}(000))$ ions [21−24]. Other two bands marked by "A" in Fig.2 can be assigned to the $A^2\Pi_{1/2}(203,\ 004)\leftarrow X^2\Pi_{1/2}(000)$ transitions, and their rotational contours are obviously different from those of $B^2\Sigma^+\leftarrow X^2\Pi$ transitions. In comparison with the $B^2\Sigma^+\leftarrow X^2\Pi_{3/2,1/2}(000)$ spectra in Fig.1 and Fig.2, the $B^2\Sigma^+\leftarrow X^2\Pi_{1/2}(001)$ spectrum in Fig.3 contains more vibrational bands of $B^2\Sigma^+(v_1v_2v_3)$.

IV. CONCLUSION

In sum, we have obtained the mass-resolved dissociation spectra of OCS^+ via $B^2\Sigma^+(v_10v_3)\leftarrow X^2\Pi_{3/2}(000)$ and $B^2\Sigma^+(v_1v_2v_3)\leftarrow X^2\Pi_{1/2}(000,\ 001)$ transitions in the wavelength range of 231−275 nm, and the spectroscopic constants of ν_1(CS stretch)=828.9 (810.4) cm^{-1}, ν_2(bend)=491.3 cm^{-1} and ν_3(CO stretch)=1887.2 cm^{-1} for $OCS^+(B^2\Sigma^+)$ are deduced. It is noticed that in the dissociation spectra the bands involving the ν_2(bend) mode of $OCS^+(B^2\Sigma^+)$, such as $B^2\Sigma^+(010)$, were observed in the $B^2\Sigma^+(v_1v_2v_3)\leftarrow X^2\Pi_{1/2}(000,\ 001)$ progressions but not in the $B^2\Sigma^+\leftarrow X^2\Pi_{3/2}(000)$ progression. This dependence of the bending ν_2 mode of $B^2\Sigma^+$ on

DOI:10.1063/1674-0068/26/03/265-269

the spin-orbit splitting of $X^2\Pi$ can be attributed to the effective K coupling between the $(000)^2\Pi_{1/2}$ and $(010)^2\Sigma^+_{1/2}$ vibronic levels of the $X^2\Pi$ state, which makes the $B^2\Sigma^+(v_1 1 v_3) \leftarrow X^2\Pi_{1/2}(000)$ transition becomes possible by borrowing the intensity from the allowed $B^2\Sigma^+(v_1 1 v_3) \leftarrow X^2\Pi((010)^2\Sigma^+_{1/2})$ transition.

V. ACKNOWLEDGEMENT

This work is supported by the National Natural Science Foundation of China (No.21073177).

[1] D. M. Hirst, Moleculer Phys. **104**, 55 (2006).
[2] B. Z. Chen, M. B. Huang, and H. B. Chang, Chem. Phys. Lett. **416**, 107 (2005).
[3] R. Frey, B. Gotchev, W. B. Peatman, H. Pollak, and E. W. Schlag, Int. J. Mass Spectrom. Ion Phys. **26**, 137 (1978).
[4] J. Delwiche, M. J. Hubin-Franskin, P. M. Guyon, and I. Nenner, J. Chem. Phys. **74**, 4219 (1981).
[5] C. R. Brundle and D. W. Turner, Int. J. Mass Spectrosc. Ion Phys. **2**, 195 (1969).
[6] B. J. Kovac, Chem. Phys. **78**, 1684 (1983).
[7] L. S. Wang, J. E. Reutt, Y. T. Lee, and D. A. J. Shirley, Electron Spectrosc. Relat. Phenom. **47**, 167 (1988).
[8] A. W. Potts and G. H. Fattahallah, J. Phys. B **13**, 2545 (1980).
[9] J. R. Appling, M. R. Harbol, R. A. Edgington, and A. C. Goren, J. Chem. Phys. **97**, 4041 (1992).
[10] S. Stimson, M. Evans, C. Y. Ng, C. W. Hsu, P. Heimann, C. Destandau, G. Chambaud, and P. J. Rosmus, J. Chem. Phys. **108**, 6205 (1998).
[11] W. W. Chen, M. Hochlaf, P. Rosmus, G. Z. He, and C. Y. Ng, J. Chem. Phys. **116**, 5612 (2002).
[12] Y. Ono, E. A. Osuch, and C. Y. Ng, J. Chem. Phys. **74**, 1645 (1981).
[13] M. Ochsner, M. Tsuji, and J. P. Maier, Chem. Phys. Lett. **115**, 373 (1985).
[14] M. Tsuji and J. P. Maier, Chem. Phys. Lett. **137**, 421 (1987).
[15] M. J. Hubin-Franskin, J. Delwiche, P. M. Guyon, M. Richard-Viard, M. Lavollee, O. Dutuit, J. M. Robbe, and J. P. Flament, Chem. Phys. **209**, 143 (1996).
[16] J. Delwiche, M. J. Hubin-Franskin, G. Caprace, P. Natalis, and D. Roy, J. Electron Spectrosc. Relat. Phenom. **21**, 205 (1980).
[17] R. Kakoschke, U. Boesl, J. Herman, and E. W. Schlag, Chem. Phys. Lett. **119**, 467 (1985).
[18] S. Morse, M. Takahashi, J. H. D. Eland, and L. Karlsson, Int. J. Mass Spectrom. **184**, 67 (1999).
[19] B. Yang, Y. Chiu, H. Fu, and S. L. Anderson, J. Chem. Phys. **95**, 3275 (1991).
[20] R. Weinkauf and U. Boesl, J. Chem. Phys. **101**, 8482 (1994).
[21] R. Weinkauf and U. Boesl, J. Chem. Phys. **98**, 4459 (1992).
[22] R. A. Morgan, A. J. Orr-Ewing, D. Ascenzi, and N. R. Michael, J. Chem. Phys. **105**, 2141 (1996).
[23] R. A. Morgan, M. A. Baldwin, D. Ascenzi, A. J. Orr-Ewing, M. N. R. Ashfold, W. J. Buma, J. B. Milan, and C. A. de Lange, Int. J. Mass Spectrom. Ion Phys. **159**, 1 (1996).
[24] B. Yang, H. E. Mohamad, and S. L. Anderson, J. Chem. Phys. **89**, 5527 (1988).
[25] C. Chang, C. Y. Luo, and K. Liu, J. Phys. Chem. A **109**, 1022 (2005).
[26] C. Chang, *Ph. D. Dissertation*, Taiwan: National Taiwan University, No. D90223014, (2005).
[27] M. Sommavilla and F. Merkt, J. Phys. Chem. A **108**, 9970 (2004).
[28] L. Zhang, J. Chen, H. Xu, J. Dai, S. Liu, and X. Ma, J. Chem. Phys. **114**, 10786 (2001).

DOI:10.1063/1674-0068/26/03/265-269